Physics Letters B 779 (2018) 107–116

Contents lists available at ScienceDirect

Physics Letters B

www.elsevier.com/locate/physletb

LHC signals of radiatively-induced neutrino masses and implications for the Zee–Babu model

Julien Alcaide, Mikael Chala *, Arcadi Santamaria

Departament de Física Tèorica, Universitat de València and IFIC, Universitat de València-CSIC, Dr. Moliner 50, E-46100 Burjassot (València), Spain

ARTICLE INFO

Article history:
Received 23 October 2017
Received in revised form 23 January 2018
Accepted 1 February 2018
Available online 5 February 2018
Editor: G.F. Giudice

Keywords:
Lepton-number violation
LHC searches
Higgs sector
Doubly-charged scalars

ABSTRACT

Contrary to the see-saw models, extended Higgs sectors leading to radiatively-induced neutrino masses do require the extra particles to be at the TeV scale. However, these new states have often exotic decays, to which experimental LHC searches performed so far, focused on scalars decaying into pairs of same-sign leptons, are not sensitive. In this paper we show that their experimental signatures can start to be tested with current LHC data if dedicated multi-region analyses correlating different observables are used. We also provide high-accuracy estimations of the complicated Standard Model backgrounds involved. For the case of the Zee–Babu model, we show that regions not yet constrained by neutrino data and low-energy experiments can be already probed, while most of the parameter space could be excluded at the 95% C.L. in a high-luminosity phase of the LHC.

1. Introduction

The standard model (SM) gives a natural and simple explanation for exactly massless neutrinos. However, neutrino oscillation data provide an irrefutable evidence of neutrino masses, which are much smaller than the rest of the fermions. Neutrino masses can be accommodated in extensions of the SM involving new particles or parametrized by non-renormalizable operators violating lepton number conservation (LN).

The most straightforward extension is obtained by adding three families of singlet right-handed neutrinos. If they have a large Majorana mass term M, LN is broken, left-handed neutrino masses are generated at tree level and their smallness can naturally be explained by the see-saw formula $m_\nu \sim v^2/M$, with v the vacuum expectation value (VEV) of the SM Higgs doublet. This is the so-called see-saw model type I [1–4] which arises in Grand Unification models like the ones based on $SO(10)$. The simplicity of the model and the fact that it appears naturally in well motivated extensions of the SM makes the see-saw type I as the most appealing explanation of neutrino masses. A more complicated extension, but richer phenomenologically, is obtained by replacing the singlet neutrinos by triplets of fermions without hypercharge (see-saw type III [5,6]). Both, type I and type III see-saws, contain only one new physics scale, the Majorana mass of the new fermions, M, and lead to the same see-saw formula. Therefore, to explain the observed tiny neutrino masses one needs an extremely large M making very difficult to test these mechanisms.[1]

Alternatively, to generate neutrino masses at tree level one can enlarge the SM with a scalar triplet with hypercharge $Y = 1$, which develops a VEV (see-saw type II [9–14]). The model contains two mass scales, the mass of the new particles, M, and a trilinear coupling which breaks explicitly LN, μ. Then, the neutrino masses are $m_\nu \sim \mu v^2/M^2$. If $\mu \sim M$ we are in a situation similar to see-saws type I and III, the scale must be very large and the model difficult to test. However, since μ is protected by symmetry (it is the only coupling in the Lagrangian that breaks LN), it can be naturally small, $\mu \ll M$. Then, M can be at the electroweak (EW) scale and the new particles could be produced at the LHC and/or give large effects in low energy experiments by virtual exchange (for instance, lepton flavor violating processes).

In the see-saws one explains the smallness of neutrino masses by introducing large mass scales as compared to the EW scale. The new heavy particles give huge loop contributions to the SM Higgs mass, which show in all its crudity the hierarchy problem of the SM. This problem can be alleviated in models in which neutrino

[1] This conclusion can be avoided if a larger number of fermions is introduced with a particular structure of the mass matrix containing different scales, as in the so-called inverse see-saw mechanism [7,8], or taking very small Yukawa couplings as in the case of Dirac neutrinos.

* Corresponding author.
E-mail address: mikael.chala@cern.ch (M. Chala).

https://doi.org/10.1016/j.physletb.2018.02.001

masses are suppressed by loop factors. For instance, if we enlarge the SM with only scalars, other than triplets with $Y = 1$, neutrino masses cannot arise at tree level. However, if LN is broken in the scalar potential, sooner or later Majorana neutrino masses will appear as radiative corrections. Typically this mechanism gives a neutrino mass formula like the see-saw type II, but suppressed by loop factors, $m_\nu \sim \frac{1}{(16\pi^2)^n}\mu v^2/M^2$, where $n = 1, 2, 3, \cdots$ is the number of loops at which the mass is generated and μ is the coupling of the potential that breaks LN. Moreover, the breaking of LN involves the simultaneous presence of several Yukawa couplings which produces further suppressions in the neutrino mass formula. With all these suppressions, the mass of the new particles, M, can be rather low even if μ is not small as compared with M. This makes these models testable in present and near future experiments.

The simplest of these models is the Zee–Babu model [15,16], which contains only two complex scalar singlets, singly and doubly charged, which we will denote as h and k respectively, and gives neutrino masses at two-loops. The model has a very rich phenomenology that has been widely studied; see for instance Refs. [17–21]. The Zee–Babu model is just a representative of a large class of interesting models which give small radiative neutrino masses by extending only the Higgs sector. Archetypes of this class of models are the Zee model [22] for masses generated at one loop (see Ref. [23] for one-loop models with leptoquarks), Refs. [15, 16,24,25] for two-loop masses (see Ref. [26] for a model with leptoquarks) and Refs. [27,28] for three-loop masses (see also [29] for a recent review and a complete list of references). These models are further motivated by the fact that, contrary to the rest of the SM interactions, departures from the SM can be plausibly hidden in the scalar sector, which is not precisely measured yet. Most of the models we shall be interested contain doubly-charged scalars,[2] which have a very rich and peculiar phenomenology.

Several experimental searches for doubly-charged scalars have been carried out at the LHC [30–35]. They all concluded with negative results. However, unlike some widespread sociological feelings, these results should not be discouraging. On the contrary, a critical assessment of these analyses reveals that they are all not sensitive to doubly-charged scalars with decays other than into same-sign leptons. Departures from this assumption have been already considered in the literature. Thus, pair-produced doubly-charged scalars decaying into W bosons [36,37] or with both W boson and leptonic decays [38] have been studied. However, no LHC study of doubly-charged scalars with exotic decays, as those arising in models of radiatively-induced neutrino masses (*e.g.* the Zee–Babu model), which are the ones that *must* really have TeV masses, has been worked out so far. In fact, the Zee–Babu model contains the coupling $\mu k^{++}h^-h^-$, which is essential in the generation of neutrino masses and can lead to the decay $k^{\pm\pm} \to h^\pm h^\pm$. The aim of this paper is to make progress in this direction.

With this spirit, in section 2 we motivate several doubly-charged scalar exotic decay modes that will be subsequently studied in section 3. In this section we highlight the most promising LHC observables and signal regions defined out of them to test doubly-charged scalars in a variety of realistic models of neutrino masses. Given the technical difficulties of determining the SM background with good accuracy,[3] and the fact that our proposed analysis can be eventually used to study prospects for many other scenarios, we also provide background estimations for each of the signal categories considered in this work in appendix A. In section 3, we investigate the reach of this search for the famous Zee–Babu model [15,16], in (very broad) parameter space regions not yet constrained by neutrino data. Finally, we conclude in section 5.

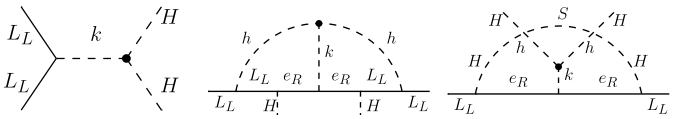

Fig. 1. Feynman diagrams inducing Majorana neutrino masses in the EW phase in the see-saw type II (left), the Zee–Babu model (center) and the model of Ref. [28] (right). H stands for the Higgs doublet. The black dot shows that, provided it is kinematically allowed, k decays into final states other than same-sign leptons (the neutrino masses would vanish otherwise).

2. Exotic decays of doubly-charged scalars

We will restrict ourselves to SM extensions with only uncolored scalars[4] with electric charged, at most, $Q = 2$. We will denote by k the doubly-charged scalar whose decays we are interested in. In addition, we will call χ, h and S any additional doubly-charged, singly-charged or neutral scalar, respectively. Besides the leptonic decay of k, $k^{\pm\pm} \to \ell^\pm\ell^\pm$, new decay modes are typically present. In fact, k must also couple linearly to non-leptonic fields, because otherwise it would not break LN and therefore would not generate (LN violating Majorana) masses for the neutrinos. (Note that Dirac masses can not be induced by purely scalar extensions of the SM.) In particular, the following k decay modes take place in a variety of models:

$\mathbf{k^{\pm\pm} \to W^\pm W^\pm}$. It appears even in the simplest model, the see-saw type II, which extends the Higgs sector with an $SU(2)_L$ triplet with $Y = 1$; see the left panel of Fig. 1 (the W bosons are hidden in the longitudinal components of the Higgs doublet). Provided the VEV of the neutral component of this triplet is large enough, k decays predominately into gauge bosons. As an example, for a k mass $m_k \sim 500$ GeV, and assuming the neutrino masses to fulfill $\sum m_{\nu_i}^2 = 0.1^2$ eV^2, the triplet VEV has to be only above ~ 0.0001 GeV [40]. (Note that this value does not spoil the ρ parameter bound on this VEV, $\lesssim$ few GeV.)

Finally, this decay mode appears also naturally in extended composite Higgs models [37], which are further motivated by the gauge-hierarchy problem.

$\mathbf{k^{\pm\pm} \to h^\pm h^\pm, h^\pm \to \ell^\pm \nu}$. Most importantly, it is the only other possible k decay that occurs in the Zee–Babu; see the center panel of Fig. 1.

$\mathbf{k^{\pm\pm} \to h^\pm h^\pm, h^\pm \to W^\pm S}$. It has been shown to occur in models where both h and S are odd under a $\mathbb{Z}_2$ symmetry, while k is even; see *e.g.* Ref. [27]. A more recent example is given by the model of Ref. [28]; see Fig. 1 right panel. Contrary to the first one, in this model h is part of an $SU(2)_L$ triplet with $Y = 1$ (instead of a doublet with $Y = 1/2$) containing an additional doubly-charged scalar χ. Consequently, we can also find the following decay mode:

$\chi^{\pm\pm} \to \mathbf{k^{\pm\pm} S}, \mathbf{k^{\pm\pm}} \to \ell^\pm\ell^\pm$. An interesting aspect of this channel is that, for given χ and S masses, it can sensibly *strengthen* the

[2] One prominent exception is the Zee model [22], which contains only singly-charged scalars.

[3] As we emphasize further in section 3, three main challenges affect the generation of the dominant SM backgrounds leading to multi-lepton final states. *(i)* Most of the SM processes contain several particles in the final state. *(ii)* A large fraction of the background is due to charge miss-identification of electrons and positrons coming from huge SM processes such as Z + jets. *(iii)* Reaching the TeV region of mass distributions (and other observables with energy dimensions) suggest that NLO-accurate computations must be performed.

[4] We remark that all colored scalars with renormalizable couplings to SM fields are flavor-violating, and hence severely constrained; see *e.g.* reference [39].

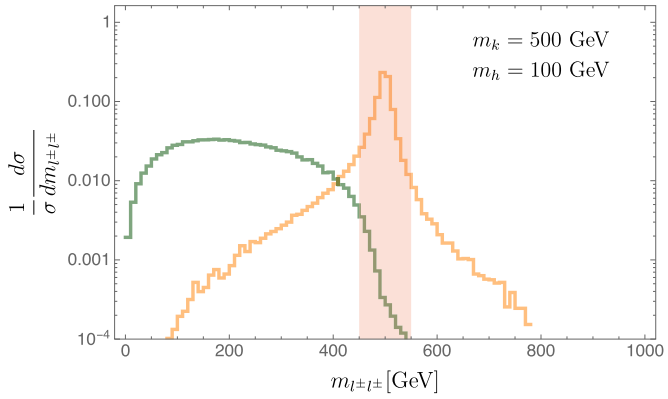

Fig. 2. Orange: Invariant mass distribution of each pair of two same-sign leptons in events $pp \to k^{++}k^{--}$ with $k^{\pm\pm} \to \ell^\pm\ell^\pm$. Green: Same as before but with $k^{\pm\pm} \to h^\pm h^\pm, h^\pm \to \ell^\pm\nu$. Red: cut imposed by the experimental collaboration [35]. m_k and m_h have been set to 500 and 100 GeV, respectively. (For interpretation of the references to color in this figure legend, the reader is referred to the web version of this article.)

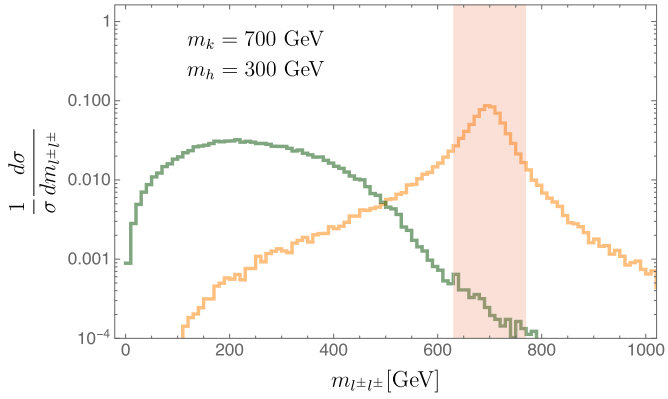

Fig. 3. Same as Fig. 2 but for $m_k = 700$ GeV and $m_h = 300$ GeV. (For interpretation of the references to color in this figure, the reader is referred to the web version of this article.)

bounds on m_k coming from current searches for doubly-charged scalars.

Finally, despite being potentially present, we do not consider cascade decays of k via emission of W bosons. As we will comment below, these are very hard to constrain experimentally.

3. Search strategy

Both the ATLAS and the CMS collaborations have developed a large amount of searches for doubly-charged scalars. These include analyses of the total collected luminosity at 7 [31,32], 8 [41,42] and 13 [34,35,43] TeV of center of mass energy. However, they are all inspired by the see-saw type II and therefore look for final states containing pairs of same-sign leptons reconstructing a narrow invariant mass. This requirement is only (and slightly) relaxed in final states with taus. Consequently, doubly-charged scalars with exotic decays can easily be missed. As an example, we compare in Figs. 2 and 3 the invariant mass distribution of the two same-sign lepton pairs resulting from the decay of doubly-charged scalars into $\ell^\pm\ell^\pm$ (orange) and $h^\pm h^\pm$ with $h^\pm \to \ell^\pm\nu$ (green). Clearly, the narrow cut removes most of the signal in this latter case.

Moreover, the interplay between different variables such as the invariant mass of pairs of leptons or the missing energy is never fully exploited. In addition, other analyses, and in particular searches for Supersymmetry in multi-lepton final states, are also non constraining (even for small doubly-charged scalar masses). We have tested this by means of `CheckMATE v2` [44], which implements, among others, searches for gluinos in final states with two same-sign leptons or three leptons, jets and missing energy [45]. A last analysis that might be sensitive to the signals we are interested in is given by the CMS search for the seesaw type-III in multi-lepton final states [46]. Again, this search is of narrow scope. Among the characteristics that make it not suitable to explore generic doubly-charged scalars we find that it focuses on final states with same-flavor opposite-sign leptons. For models such as the Zee–Babu, where the doubly-charged scalar can produce equally muons or electrons, this requirement kills half of the signal. Furthermore, final states with only two light leptons, which are abundant in the models of interest, are disregarded. In any case, that CMS paper does not provide detailed information (*e.g.* number of background events in each signal category), and so a proper estimation of its (presumably limited) reach to these models can not be precisely stated. To the best of our knowledge, no other multi-lepton analysis with the latest data has been made public yet.

As things stand, new analyses are necessary to fully explore models of radiatively-induced neutrino masses. With the aim of being able to test different scenarios (though still focusing on neutrino models[5]), we propose a broad scope search containing several signal regions and categories.

They all contain several same-sign leptons. One of the main challenges of this kind of analysis is the correct estimation of the background, which originates mainly from the charge misidentification of electrons. This requires time-consuming simulations of SM processes with many particles in the final state. Consequently, given the numerous signal regions that we work out in the next section, our background estimation will be valuable for many LHC studies of particles producing same-sign lepton events.

3.1. New signal regions

Prior to the selection of events, the relevant physical objects are constructed in the following way. Electrons (muons) are defined to have $p_T^\ell > 20$ (10) GeV and $|\eta_\ell| < 2.5$ (2.6). Jets are clustered using the anti-k_t algorithm with $R = 0.4$. They are defined by $p_T^j > 20$ GeV and $|\eta_j| < 2.4$. Despite their small phenomenological relevance, we have also fixed the b-tagging efficiency to 0.7 and the τ-tagging efficiency to 0.5. Of major importance is the probability of an electron (positron) to be identified as a positron (electron). Following Ref. [34] we estimate it by $P(|\eta_\ell|, p_T^\ell) = f(|\eta_\ell|)\sigma(p_T^\ell)$ with

$$f(x) = \begin{cases} 0.03 & \text{if} \quad 0 < x < 0.4, \\ 0.04 & \text{if} \quad 0.4 < x < 0.8, \\ 0.08 & \text{if} \quad 0.8 < x < 1.1, \\ 0.15 & \text{if} \quad 0.8 < x < 1.1, \\ 0.3 & \text{if} \quad 1.1 < x < 1.4, \\ 0.6 & \text{if} \quad 1.4 < x < 1.7, \\ 0.7 & \text{if} \quad 1.7 < x < 1.9, \\ 1 & \text{if} \quad 2.1 < x < 2.3, \\ 2 & \text{if} \quad x > 2.3, \end{cases} \tag{1}$$

and

$$\sigma(x) = \begin{cases} 0.02 & \text{if} \quad x < 70, \\ 0.035 & \text{if} \quad 70 < x < 100, \\ 0.05 & \text{if} \quad x > 100. \end{cases} \tag{2}$$

[5] Despite being interesting, inclusive searches looking "everywhere" *without* any theoretical biased, such as the model-independent analysis of Ref. [47], are not very efficient in the search for new physics.

Table 1
Backgrounds, cross sections and numbers of generated Monte Carlo events.

	σ [pb]	# MC events
Drell–Yan	220 ± 20	10^8
$t\bar{t}$	660 ± 70	10^8
WW	102 ± 4	10^7
WZ	45 ± 2	10^6
ZZ	13.6 ± 0.5	10^6
WWW	0.21 ± 0.01	10^6
WWZ	0.17 ± 0.01	10^6
WZZ	0.057 ± 0.004	10^6
ZZZ	0.014 ± 0.001	10^6
$t\bar{t}W$	0.59 ± 0.06	10^6
$t\bar{t}Z$	0.76 ± 0.09	10^6

Throughout the text, we will refer to electrons and muons simply as *leptons*, while taus will be excluded from this definition. Only events with at least two same-sign leptons are selected. Out of this sample, we define three orthogonal signal regions (SRs), containing two, three and four leptons, respectively.

SR 1: inspired by the recent ATLAS analysis of Ref. [34], it contains events with two leptons. If more than two same-sign leptons are present, only that pair with the highest invariant mass is considered for computing the observables defined below.

SR 2: inspired by the recent CMS analysis of Ref. [35], it contains events with exactly three leptons, with exactly two of opposite sign.

SR 3: inspired by the same CMS analysis, it contains events with exactly two positive and two negative leptons.

We further consider the following observables. 1) S_T, defined as the scalar sum of the p_T of all leptons in the signal region. 2) The invariant mass of each same-sign lepton pair, $m_{\ell^\pm\ell^\pm}$. 3) The transverse mass of each same-sign lepton pair, as well as the one of the third lepton in SR 3. We will denote both collectively by m_T. Following Ref. [37], we define the former by

$$m_T^2 = \left[\sqrt{(p_T^{\ell^\pm\ell^\pm})^2 + m^2_{\ell^\pm\ell^\pm}} + E_T^{\rm miss}\right]^2 \tag{3}$$

$$- \left[p_x^{\ell^\pm\ell^\pm} + E_x^{\rm miss}\right]^2 - \left[p_y^{\ell^\pm\ell^\pm} + E_y^{\rm miss}\right]^2 , \tag{4}$$

where $E^{\rm miss}$ stands for the missing energy. 4) The transverse mass, m_{T2}, defined as

$$m_{T2} = \min_{\mathbf{q}_T}\left\{\max\left[p_T^{L_1} E_T^{\rm miss} - \mathbf{p}_T^{L_1}\cdot\mathbf{q}_T, \right.\right. \tag{5}$$

$$\left.\left. p_T^{L_2} E_T^{\rm miss} - \mathbf{p}_T^{L_2}\cdot(\mathbf{E}_T^{\rm miss} - \mathbf{q}_T)\right]\right\} . \tag{6}$$

In SR1, L_1 and L_2 are given by the harder and the softer lepton, respectively. In SR2, L_1 stands for the vectorial sum of the two same-sign leptons, while L_2 is given by the third one. In SR3, L_1 represents the vectorial sum of the two positive charged leptons, and L_2 the vectorial sum of the two negative ones.

For each SR, and for each observable $O = m_{\ell^\pm\ell^\pm}$, m_T, m_{T2}, we consider 81 different categories defined by $S_T > X$ and $O > Y$ with $X, Y = 100, 200, \ldots, 900$ GeV. In accord with Ref. [35], we consider the following dominant backgrounds: Drell–Yan with $m_{\ell^+\ell^-} > 100$ GeV, $t\bar{t}$, WZ, WW, ZZ, WWW, WWZ, WZZ, ZZZ, $t\bar{t}W$, $t\bar{t}Z$. Background events are generated at NLO in α_s with `MadGraph v5` [48]. Initial and final state radiation and showering is performed by `Pythia v6` [49]. The cross sections of all relevant backgrounds are shown in Table 1. The uncertainty due to the choice of scale is also shown. Finally, we also provide the number of generated Monte Carlo events.

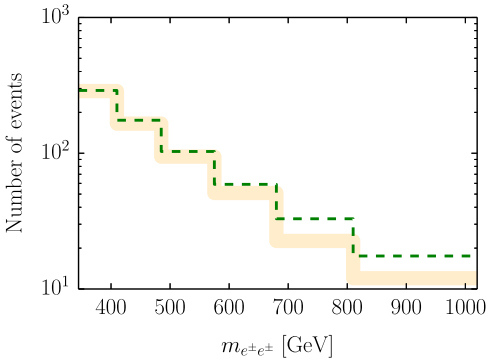

Fig. 4. Number of events with $m_{e^\pm e^\pm} > 345, 410, 485, 575, 680, 810, 1020$ GeV after the preselection cuts of Ref. [34]. The orange solid line stands for our result, while the green dashed one corresponds to the results provided by the ATLAS collaboration. The small discrepancy at large invariant masses is not relevant in practice, because the SM background is almost negligible in that region. (For interpretation of the references to color in this figure legend, the reader is referred to the web version of this article.)

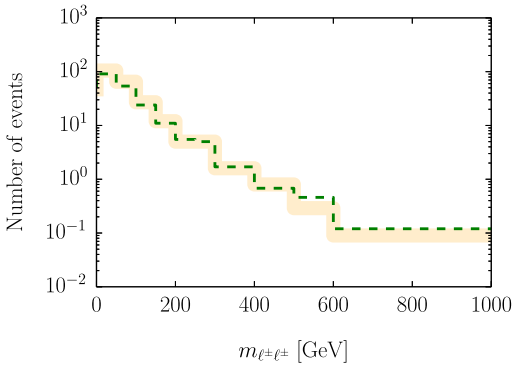

Fig. 5. Event distribution for $m_{\ell^\pm\ell^\pm}$ after the preselection cuts of Ref. [35]. The orange solid line stands for our result, while the green dashed one corresponds to the results provided by the CMS collaboration. (For interpretation of the references to color in this figure legend, the reader is referred to the web version of this article.)

In order to validate the goodness of our Monte Carlo generation as well as the appropriateness of Eqs. (1) and (2), we recast the analysis of Ref. [34] and compare the distribution of $m_{e^\pm e^\pm} > 345, 410, 485, 575, 680, 810$ and 1020 GeV provided by the experimental collaboration with that obtained by us. For this goal, we use homemade routines based on `MadAnalysis v5` [50] and `ROOT` [51]. The result is depicted in Fig. 4.

We also compare the distribution of $m_{\ell^\pm\ell^\pm}$ given in Ref. [35] with ours; it can be seen in Fig. 5. Clearly, our results are in perfect agreement with those provided by the experimental collaborations. Moreover, we have checked that the contribution of each background in Table 1 to the total SM expectation agrees with that reported by both ATLAS and CMS. Consequently, we have computed the number of expected background events in each of the categories mentioned above. These are listed in Tables 2, 3, 4, 5, 6, 7, 8, 9 and 10 in the appendix A.

3.2. Applications

Based on this information, we can estimate the reach of current data to several signals mediated by doubly-charged scalars. Let us start considering the standard case $k^{\pm\pm} \to \ell^\pm\ell^\pm$. This is the only one that has been considered in experimental analyses so far; it will allow us to further validate our approach. We focus on pair-production of doubly-charged scalars. As a matter of fact, this

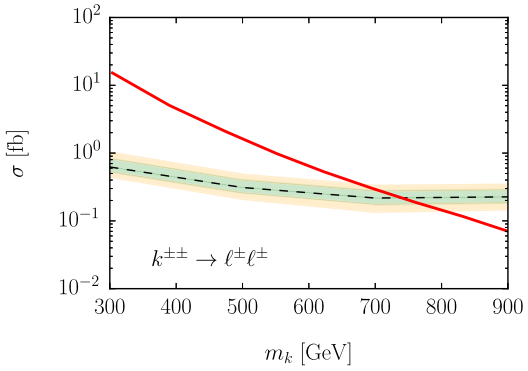

Fig. 6. Bounds on the cross section of pair-produced k decaying into same-sign leptons (dashed black line). The green and orange regions show the 1 σ and 2 σ uncertainties. We have fixed $\mathcal{L} = 35$ fb^{-1}. The theoretical cross section in the triplet case is also shown for reference (solid red line). Other model details are such that k decays only into light leptons with narrow width. (For interpretation of the references to color in this figure legend, the reader is referred to the web version of this article.)

channel is always present, while associated production is absent in many models; see section 2.

We implement the relevant interactions in `Feynrules v2` [52]. We generate signal events using `MadGraph v5` at LO in α_s, using again `Pythia v6` as parton shower. We then estimate the number of signal events in each of the categories defined above for $\mathcal{L} = 35$ fb^{-1}. (We restrict to this value because no experimental analysis with more data is still publicly available.) We subsequently look for those three categories that give the largest sensitivity defined as $S/\sqrt{B}$ in SR1, SR2 and SR3, respectively. (Obviously, in the present four-lepton case, the sensitivity is by far driven by the categories with $m_{\ell^\pm\ell^\pm} \gtrsim m_{k^{\pm\pm}} - 100$ GeV in SR3.)

These three categories are orthogonal, meaning that no single event can belong to more than one of them. We can therefore simultaneously consider these three independent categories to analyze to what extent the signal is compatible with the observed data given the SM predictions of appendix A. To this aim, we adopt the CL$_s$ method [53]. The corresponding statistic is computed using `MCLimits` [54], which takes also into account the systematic uncertainty due to the finite number of generated Monte Carlo events. On top of it, we include a systematic uncertainty in the background normalization of 10%. For each value of $m_k = 300, 500, 700, 900$ GeV, we estimate the lowest cross section that can be excluded at the 95% C.L. using this procedure. Exclusions for intermediate masses are obtained by linear interpolation.

The results are depicted by the black dashed line in Fig. 6. The shaded green and orange regions represent the 1σ and the 2σ error bands. For concreteness, we superimpose the theoretical cross section predicted when k belongs to an EW triplet. Note that this quantum number fixes completely the pair-production strength, independently of other model details (*e.g.* concrete couplings or possible further particles). These are relevant for neutrino masses, but we will discuss this interplay only in section 3.2, where we consider concrete models. The results shown in Fig. 6 are in very good agreement with those presented in the experimental works of Refs. [34] and [35]. As things stand, masses as large as $m_k \sim 700$ GeV are excluded in this channel by using current data. Note however that these are significantly weakened in models in which k is an $SU(2)_L$ singlet, whose production cross section is roughly a factor of 2 smaller.

One can easily derive approximate prospects for a larger luminosity, by scaling the cross section bound by $\sqrt{35\text{ fb}^{-1}/\mathcal{L}}$. Thus, the cross section limit at large masses goes down one order of magnitude for $\mathcal{L} = 3$ ab^{-1}. The lower limit on the triplet masses turns out to be in this case ~ 1.1 TeV. We note, however, that some corrections to this result might be needed, given the limited statistic of some Monte Carlo samples (see Table 1) for large luminosities.

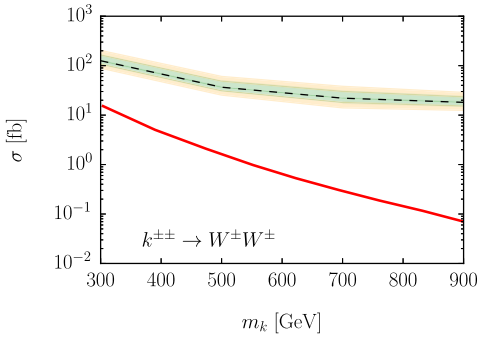

Fig. 7. Same as Fig. 6 but for $k^{\pm\pm} \to W^\pm W^\pm$. (For interpretation of the colors in this figure, the reader is referred to the web version of this article.)

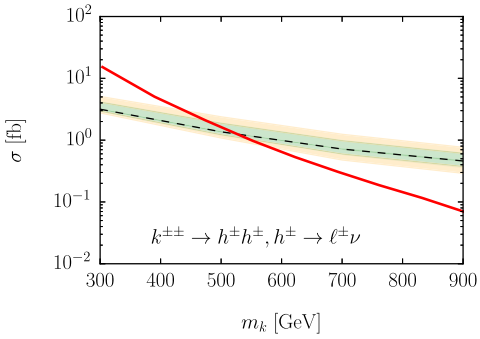

Fig. 8. Same as Fig. 6 but for $k^{\pm\pm} \to h^\pm h^\pm, h^\pm \to \ell^\pm\nu$. We fixed $m_h = m_k/2.5$. (For interpretation of the references to color in this figure, the reader is referred to the web version of this article.)

We repeat this exercise for the different signals commented in section 2, to which current analyses, relying on a narrow cut on the invariant mass of any pair of same-sign leptons, are not sensitive at all. The first such a signal appears when $k^{\pm\pm} \to W^\pm W^\pm$, what can happen also in the see-saw type II. We still restrict to the pair-production mode. (Note that the associated production channel is not necessarily present even in these models with this decay; see for example Ref. [55].) The most sensitive categories are those with $m_T, S_T \gtrsim 100$–300 GeV in SR1, $m_T \gtrsim 100$–300 GeV and $S_T > 400$–600 GeV in SR2 and the ones with $m_{\ell^\pm\ell^\pm} \gtrsim 100$–$300$ GeV and $S_T \gtrsim 600$ GeV in SR3. In this case, we have checked that the combination of the three categories with two, three and four leptons improve the sensitivity of LHC data by almost an order of magnitude with respect to that obtained using only the most sensitive category. Even so, the presence of W bosons in the final state makes this channel almost unaccessible with current data; see Fig. 7. In the long term, instead, masses up to $m_k \sim 400$ GeV might be probed. Analyses specifically dedicated to this channel in composite Higgs models could improve over this result; see Ref. [37].

Using this same broad-scope strategy, we analyze the LHC reach for pair-produced doubly-charged scalars decaying into exotic channels (with 100% branching ratio). The results are shown in Figs. 8, 9 and 10. Note that the theoretical red line should be only seen as a reference cross section, which is the LO k pair-production cross section when k belongs to an EW triplet. In particular, we note that although BR($k^{\pm\pm} \to h^\pm h^\pm$) = 1 (Figs. 8, 10) might be

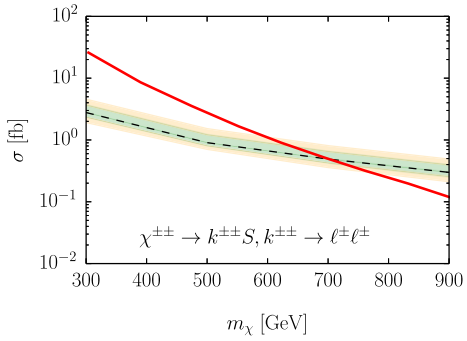

Fig. 9. Same as Fig. 6 but for $\chi^{\pm\pm} \to k^{\pm\pm} S, k^{\pm\pm} \to \ell^\pm \ell^\pm$. The red curve represents in this case the theoretical pair-production cross section for χ, assuming the latter belongs to an EW triplet. We fix $m_k = m_S = m_\chi/2.5$. (For interpretation of the references to color in this figure, the reader is referred to the web version of this article.)

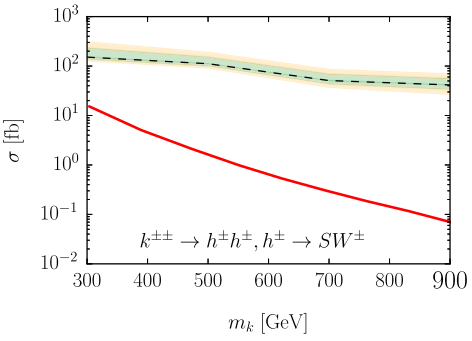

Fig. 10. Same as Fig. 6 but for $k^{\pm\pm} \to h^\pm h^\pm, h^\pm \to SW^\pm$. We fix $m_h = m_k/2.5, m_S = m_k/4$. Three body decays via off-shell W are considered when necessary. (For interpretation of the references to color in this figure, the reader is referred to the web version of this article.)

possible in the aforementioned triplet case, it would require large trilinear couplings and hence conflict with neutrino masses. However, it arises naturally if neutrino masses are generated radiatively. On another hand, the decay depicted in Fig. 9 arises only in more involved models, as commented in section 2. We see that cascade decays with W bosons in the final state are still hard to tag. It can be then easily understood that decay chains with emissions of soft W bosons are also very unconstrained. Therefore, a large parameter space of models giving these decays is perfectly allowed by collider data. On the contrary, the pair-production of $k^{\pm\pm}k^{\mp\mp}$ with the subsequent decay of $k^{\pm\pm} \to h^\pm h^\pm$ is very constrained. The most sensitive signal categories in this respect are those with $m_{T2} \sim S_T \gtrsim m_k/2$ in SR1 and those with $m_T \sim S_T \gtrsim m_k/2$ in SR2 and SR3.

Likewise, $\chi^{\pm\pm} \to k^{\pm\pm} S$ with S stable (*i.e.* missing energy) and $k \to \ell^\pm \ell^\pm$ is almost as constrained as the standard pair-production of doubly-charged scalars with leptonic decays. Thus, in models in which this production mode is present, constraints on k can be significantly altered with respect to those obtained using standard searches for k alone (see Fig. 11) because the latter is more copiously produced.

4. Implications for concrete models

In concrete models, the doubly-charged particles can decay into several different channels, and so the bounds on different parameter space points can not be read from the plots above. Instead, the full process of comparing signal, background and data outlined in section 3.2 must be done. Note, however, that the background,

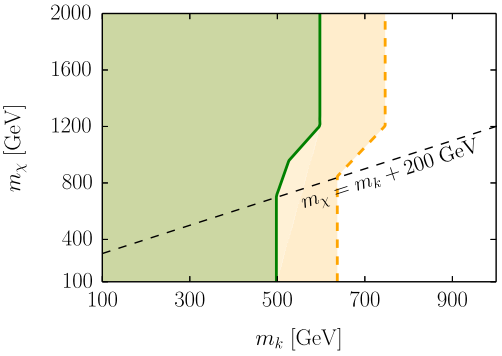

Fig. 11. Excluded region for a model containing an $SU(2)_L$ singlet $k^{\pm\pm}$ decaying into $\ell^\pm \ell^\pm$ as well as a doubly-charged component of a $Y = 1$ $SU(2)_L$ triplet, $\chi^{\pm\pm}$, decaying mostly into $\kappa^{\pm\pm}$ and a neutral scalar S when kinematically accessible (dashed orange line). The bounds on m_k are ~ 100 GeV above those obtained assuming the presence of this particle alone. We also show the bounds when $k^{\pm\pm}$ decays mostly into $\ell^\pm \tau^\pm$ (green solid line), as suggested by the recent proposed model of reference [28]. For consistency with this model, we have in both cases assumed the mass of S to be 200 GeV. (For interpretation of the references to color in this figure legend, the reader is referred to the web version of this article.)

which is the most complicated and time-consuming task in this respect, does not need to be computed again. It can be just taken from the tables in appendix A. We illustrate this procedure in the Zee–Babu model. It has been previously considered in several references [15–21]. All of them assumed that the exotic decays of the doubly-charged scalars were impossible to tag at the LHC.

4.1. The Zee–Babu model

The Zee–Babu model extends the SM scalar sector with two $SU(2)_L$ singlets, h and k, with hypercharges $Y = 1$ and $Y = 2$, respectively. The relevant Lagrangian for our discussion reads

$$L = L_{\rm SM} + f^{ab}\overline{\tilde{L}_{aL}} L_{Lb} h^+ + g^{ab}\overline{e^c_a} e_b k^{++} - \mu k^{++} h^- h^- + \text{h.c.} + \cdots \tag{7}$$

where $L_{\rm SM}$ stands for the SM Lagrangian and L_{aL}, ℓ_a with $a = 1, 2, 3$ are the first, second and third generation SM lepton doublets and singlets, respectively, and $\tilde{L}_L = i\sigma_2 L^c_L$ with σ_2 the second Pauli matrix. Overall, the model depends only on the antisymmetric (resp. symmetric) dimensionless couplings f_{ab} (resp. g_{ab}), the physical masses of the new scalars, namely m_k and m_h and the dimensionless parameter κ defined by $\mu = \kappa \min\{m_h, m_k\}$. The relevant decay widths read

$$\Gamma_{k^{\pm\pm} \to \ell^\pm_a \ell^\pm_b} = \frac{|g_{ab}|^2}{4\pi\,(1+\delta_{ab})} m_k\,, \tag{8}$$

and

$$\Gamma_{k^{\pm\pm} \to h^\pm h^\pm} = \frac{1}{8\pi}\left(\frac{\mu}{m_h}\right)^2 m_k \sqrt{1 - \frac{4m_h^2}{m_k^2}}\,. \tag{9}$$

Naturalness arguments, together with the requirement that no charge-breaking global minimum is developed by the potential, imply that $\kappa \lesssim 4\pi$. Neutrino oscillation data and low-energy constraints restrict the allowed parameter space. We consider two large regions permitted by current experiments, depending on whether the neutrino mass hierarchy is normal (NH) or inverted (IH) [20,21].

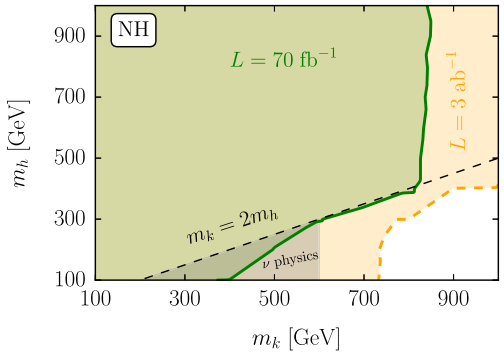

Fig. 12. Excluded regions in the plane $m_k - m_h$ in the NH in the Zee–Babu model. See the text for details. (For interpretation of the references to color in this figure, the reader is referred to the web version of this article.)

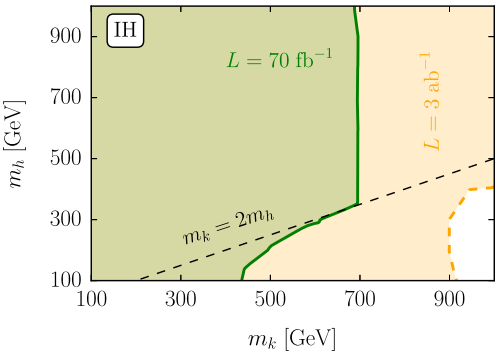

Fig. 13. Excluded regions in the plane $m_k - m_h$ in the IH in the Zee–Babu model. See the text for details. (For interpretation of the colors in this figure, the reader is referred to the web version of this article.)

4.1.1. Normal hierarchy

According to neutrino data, $g_{11} \sim g_{22} \sim 0.1 \gg g_{12}$, g_{13}, g_{23}, g_{33}. The region $m_k < 2m_h$ is allowed for $m_k > 400$ (resp. 600) GeV if $\kappa \sim 4\pi$ (resp. 5). The measured values of the neutrino mixing angles fix $f_{12} \sim f_{13} \sim f_{23}/2$. An overall scale of $f \sim 0.01$ is in agreement with $\mu \to e\gamma$ bounds. Accordingly, we consider the following values:

$$g_{11} = g_{22} = 0.1, g_{12} = g_{13} = g_{33} = 0.001,$$
$$f_{12} = f_{13} = 0.01, f_{23} = 0.02, \kappa = 5. \quad (10)$$

As a result, k decays mainly into leptons (for $m_k < 2m_h$), while h decays into a lepton and a neutrino around 60% of times and, to a lesser extent ($\sim$ 40%), into a tau and a neutrino. Thus, for $m_k > 2m_h$, the pair-production of doubly charged scalars give rise to two, three, and four-lepton events in 35%, 30% and 15% of the cases, respectively. Being 0 and 1-lepton events weird, our search strategy can then capture most of the signal. The scalar widths are small enough so that the narrow-width approximation holds. Consequently, we proceed as follows. We vary m_k and m_h in the range 100, 200, ..., 1000 GeV. For each pair, and having fixed all couplings to the values mentioned before, we compute Monte Carlo events and estimate the efficiency (ϵ) for selecting events in each of the categories described in previous sections. The number of expected signal events in each category for a given luminosity ($\mathcal{L}$) can then be computed as

$$N = \sigma(pp \to k^{++}k^{--}) \times \mathcal{L} \times \epsilon\,. \quad (11)$$

Then, we compare again the three most sensitive categories (one for each SR) with the corresponding SM background. The results are shown in Fig. 12. The grey triangle at the bottom of the plot is already excluded by neutrino and low-energy data. The green region enclosed by the solid green line is the area that can be excluded using the already collected luminosity $\mathcal{L} = 70$ fb^{-1} (counting 35 for each experiment, ATLAS and CMS). It is worth noting that, if we take $\kappa > 5$, the triangle excluded by neutrino data goes down to 400 GeV. Consequently, current LHC data can already constrain regions not bounded before by other experiments. Likewise, the orange region enclosed by the dashed orange line is the region that can be excluded in a high-luminosity phase of the LHC with $\mathcal{L} = 3000$ fb^{-1}. Doubly-charged scalar masses as large as 1 TeV could be probed for $k^{\pm\pm} \to \ell^\pm\ell^\pm$, but also in exotic decays.

4.1.2. Inverted hierarchy

The IH parameter space of the Zee–Babu model is very constrained by neutrino data, being m_k and m_h out of the LHC reach for most values of ϕ and δ. These parameters stand for the physical Majorana and Dirac phases in the PMNS matrix, respectively. (Note that, in the Zee–Babu model, one of the neutrinos is massless.) However, these bounds are significantly weakened if $\phi \sim \delta \sim \pi$, and even smaller for large values of κ. For definiteness, we take

$$g_{11} = g_{23} = 0.1,\ g_{12} = g_{22} = g_{13} = g_{33} = 0.0001, \quad (12)$$
$$f_{12} = 0.1,\ f_{13} = -0.1,\ f_{23} = 0.01,\ \kappa = 5. \quad (13)$$

These values are allowed by current data, even for small values of $m_k, m_h \sim 100$ GeV [21]. We emphasize that there is very small room for variations in this hierarchy of couplings. Moreover, although $\mathcal{O}(1)$ modifications in their absolute values might be in principle allowed, the expected scalar branching ratios, and therefore the LHC phenomenology, would remain the same. We proceed as in the NH case and test which region of the $m_k - m_h$ plane can be probe with current and future LHC data. The result is shown in Fig. 13. The smaller region for $m_k < 2m_h$ in comparison with the NH case is due to the smaller k branching ratio into leptons. Again, there are non-previously bounded regions that can be excluded with the current LHC data, even for $m_k > 2m_h$. Likewise, masses in the TeV region could be tested with future analyses.

5. Conclusions

We have argued that current LHC analyses can not probe doubly-charged scalars with exotic decays, as those arising in models of radiatively induced neutrino masses. Novel searches, as the ones proposed in this article, combining different signal regions and observables, are however sensitive to these particles. Thus, masses as large as $\gtrsim 500$ GeV can be accessed with current LHC data for doubly-charged scalars k decaying as $k^{\pm\pm} \to h^\pm h^\pm$, with $h^\pm \to \ell^\pm\nu$. These numbers are only slightly smaller than those for doubly-charged scalars decaying into pairs of same-sign leptons. This result has important implications for concrete scenarios, most importantly the Zee–Babu model. In particular, we have shown that parameter space regions of this model not yet constrained by neutrino and low-energy experiments can be tested with current LHC data, while much larger regions could be excluded at the 95% C.L. in a high-luminosity phase.

Conversely, models in which k decays predominately via the emission of W bosons are by far less constrained.

In any case, our results (most importantly the selection of signal regions and observables, as well as the precise determination of the SM background) can be applied to very different models of neutrino masses. Therefore, we expect that this work will be of interest for many forthcoming studies.

Acknowledgements

This work is partially supported by the Spanish MINECO under grant FPA2014-54459-P, by the Severo Ochoa Excellence Program under grant SEV-2014-0398 and by the "Generalitat Valenciana" under grant GVPROMETEOII2014-087. MC thanks the MITP for hospitality during the completion of this work.

Appendix A. Tables

The number of background for an integrated luminosity of $\mathcal{L} = 13.9\ \text{fb}^{-1}$ in the different categories of SR1, SR2 and SR3 are shown in Tables 2, 3 and 4, Tables 5, 6 and 7 and Tables 8, 9 and 10, respectively.

Table 2
S_T versus $m_{\ell\ell}$ in SR1.

$m_{\ell\ell} \setminus S_T >$ [GeV]	100	200	300	400	500	600	700	800	900
100	13000	2000	570	180	76	34	16	7	4.2
200	2700	1600	530	180	72	33	15	7	4.2
300	900	700	470	170	70	32	14	6.7	4.1
400	370	320	250	150	65	31	14	6.7	4.1
500	180	160	130	96	61	29	13	6.7	4
600	89	84	72	58	41	27	13	6.5	4
700	46	45	40	34	24	17	12	6.3	4
800	26	26	25	20	16	12	9	5.6	3.9
900	16	16	15	14	11	7.8	6.5	5.2	3.7

Table 3
S_T versus m_T in SR1. The cut on m_T applies to the two reconstructed transverse masses.

$m_T \setminus S_T >$ [GeV]	100	200	300	400	500	600	700	800	900
100	14000	2000	580	190	76	34	16	7	4.2
200	5100	1800	550	180	74	33	15	7	4.2
300	1600	1100	520	170	72	32	15	6.7	4.1
400	630	510	340	170	69	32	14	6.7	4.1
500	290	250	200	120	66	30	14	6.7	4.1
600	140	130	110	76	51	29	13	6.7	4.1
700	73	70	61	48	32	21	13	6.7	4
800	42	41	38	32	24	16	11	6.4	4
900	25	25	24	22	17	12	8.7	6	3.9

Table 4
S_T versus m_{T2} in SR1.

$m_{T2} \setminus S_T >$ [GeV]	100	200	300	400	500	600	700	800	900
100	19	5.5	1.7	0.65	0.2	0.11	0.063	0.056	0.047
200	1.1	0.97	0.55	0.21	0.08	0.051	0.036	0.031	0.02
300	0.19	0.19	0.17	0.058	0.047	0.03	0.02	0.02	0.017
400	0.035	0.035	0.034	0.034	0.024	0.021	0.022	0.02	0.017
500	0.021	0.021	0.021	0.021	0.021	0.018	0.017	0.017	0.017
600	0.018	0.018	0.018	0.018	0.018	0.018	0.017	0.017	0.017
700	0.017	0.017	0.017	0.017	0.017	0.017	0.017	0.017	0.017
800	0.017	0.017	0.017	0.017	0.017	0.017	0.017	0.017	0.017
900	0	0	0	0	0	0	0	0	0

Table 5
S_T versus $m_{\ell\ell}$ in SR2.

$m_{\ell\ell} \setminus S_T >$ [GeV]	100	200	300	400	500	600	700	800	900
100	2200	740	240	92	42	21	11	6.3	3.9
200	570	350	160	71	35	19	9.7	6	3.8
300	180	130	85	47	26	15	8.4	5.3	3.7
400	67	57	43	30	19	12	7.4	4.7	3.3
500	30	28	22	17	12	8.5	5.2	3.7	2.9
600	14	14	11	9.6	7.3	5.6	3.7	2.8	2.2
700	6.8	6.8	6.1	5.4	4.3	3.6	2.6	2.2	1.8
800	3.6	3.6	3.5	3.3	2.7	2.4	1.9	1.8	1.4
900	2.2	2.2	2.2	2	1.5	1.4	0.98	0.91	0.9

Table 6
S_T versus m_T in SR2. The cut on m_T applies to the two reconstructed transverse masses.

$m_T \setminus S_T >$ [GeV]	100	200	300	400	500	600	700	800	900
100	840	370	140	61	30	16	8.2	5.1	3.5
200	100	92	54	30	17	10	5.8	3.9	2.7
300	22	22	19	13	8.5	5.7	3.6	2.6	1.6
400	6.7	6.7	6.6	5.8	4.1	2.8	1.9	1.4	0.96
500	2.3	2.3	2.3	2.3	1.9	1.6	1.2	1	0.64
600	0.99	0.99	0.99	0.97	0.9	0.74	0.57	0.54	0.45
700	0.42	0.42	0.42	0.42	0.42	0.41	0.39	0.39	0.32
800	0.12	0.12	0.12	0.12	0.12	0.12	0.11	0.11	0.1
900	0.049	0.049	0.049	0.049	0.049	0.049	0.049	0.05	0.045

Table 7
S_T versus m_{T2} in SR2.

$m_{T2} \setminus S_T >$ [GeV]	100	200	300	400	500	600	700	800	900
100	2400	800	250	95	43	22	11	6.4	4
200	600	370	170	76	37	19	10	6.2	3.9
300	180	140	91	51	28	16	8.9	5.5	3.7
400	69	59	44	31	20	13	7.7	4.8	3.5
500	31	28	23	17	13	8.8	5.4	3.9	3
600	15	14	11	9.8	7.5	5.8	3.9	3	2.3
700	6.9	6.9	6.2	5.5	4.4	3.7	2.7	2.3	1.9
800	3.6	3.6	3.6	3.4	2.7	2.5	1.9	1.8	1.5
900	2.2	2.2	2.2	2	1.5	1.4	1	0.94	0.93

Table 8
S_T versus $m_{\ell\ell}$ in SR3.

$m_{\ell\ell} \setminus S_T >$ [GeV]	100	200	300	400	500	600	700	800	900
100	58	44	21	10	5.2	2.9	1.5	1	0.54
200	6.8	6	5.2	4.2	3.2	2.1	1.2	0.79	0.5
300	1.5	1.5	1.4	1.2	1.1	0.85	0.64	0.49	0.31
400	0.48	0.48	0.44	0.41	0.35	0.3	0.27	0.24	0.15
500	0.15	0.15	0.15	0.15	0.15	0.13	0.13	0.13	0.073
600	0.053	0.053	0.053	0.053	0.052	0.069	0.069	0.069	0.035
700	0.052	0.052	0.052	0.052	0.051	0.051	0.051	0.051	0.017
800	0.017	0.017	0.017	0.017	0.017	0.017	0.017	0.017	0
900	0.017	0.017	0.017	0.017	0.017	0.017	0.017	0.017	0

Table 9
S_T versus m_T in SR3. The cut on m_T applies to the two reconstructed transverse masses.

$m_T \setminus S_T >$ [GeV]	100	200	300	400	500	600	700	800	900
100	65	48	23	11	5.4	3	1.6	1	0.57
200	9.4	8.5	6.8	5.2	3.6	2.3	1.3	0.87	0.52
300	2.4	2.3	2.1	1.8	1.5	1.1	0.76	0.58	0.34
400	0.78	0.78	0.75	0.69	0.55	0.42	0.37	0.32	0.18
500	0.22	0.22	0.22	0.23	0.22	0.2	0.17	0.16	0.083
600	0.1	0.1	0.1	0.1	0.094	0.12	0.11	0.11	0.047
700	0.069	0.069	0.069	0.069	0.068	0.066	0.063	0.059	0.013
800	0.037	0.037	0.037	0.037	0.037	0.037	0.037	0.034	0.0047
900	0.02	0.02	0.02	0.02	0.02	0.02	0.02	0.02	0.0024

Table 10
S_T versus m_{T2} in SR3.

$m_{T2} \setminus S_T >$ [GeV]	100	200	300	400	500	600	700	800	900
100	220	120	34	13	6.3	3.2	1.7	1.1	0.61
200	56	45	26	12	6.1	3.2	1.7	1.1	0.61
300	18	16	12	8.3	5.2	3	1.6	1.1	0.61
400	6.7	6.2	5	4.2	3.3	2.3	1.5	1.1	0.62
500	3.2	3.1	2.7	2.4	2.1	1.6	1.2	0.95	0.59
600	1.6	1.6	1.5	1.4	1.2	0.96	0.87	0.73	0.48
700	0.88	0.88	0.88	0.82	0.72	0.59	0.56	0.52	0.36
800	0.6	0.6	0.6	0.58	0.5	0.43	0.41	0.39	0.28
900	0.46	0.46	0.46	0.43	0.37	0.33	0.31	0.29	0.2

References

[1] P. Minkowski, $\mu \to e\gamma$ at a rate of one out of 10^9 muon decays?, Phys. Lett. B 67 (1977) 421–428.
[2] M. Gell-Mann, P. Ramond, R. Slansky, Complex spinors and unified theories, Conf. Proc. C 790927 (1979) 315–321, arXiv:1306.4669.
[3] T. Yanagida, Horizontal symmetry and masses of neutrinos, Conf. Proc. C 7902131 (1979) 95–99.
[4] R.N. Mohapatra, G. Senjanovic, Neutrino mass and spontaneous parity violation, Phys. Rev. Lett. 44 (1980) 912.
[5] R. Foot, H. Lew, X.G. He, G.C. Joshi, Seesaw neutrino masses induced by a triplet of leptons, Z. Phys. C 44 (1989) 441.
[6] E. Ma, D.P. Roy, Heavy triplet leptons and new gauge boson, Nucl. Phys. B 644 (2002) 290–302, arXiv:hep-ph/0206150.
[7] D. Wyler, L. Wolfenstein, Massless neutrinos in left-right symmetric models, Nucl. Phys. B 218 (1983) 205–214.
[8] R.N. Mohapatra, J.W.F. Valle, Neutrino mass and baryon number nonconservation in superstring models, Phys. Rev. D 34 (1986) 1642.
[9] W. Konetschny, W. Kummer, Nonconservation of total lepton number with scalar bosons, Phys. Lett. B 70 (1977) 433–435.
[10] T.P. Cheng, L.-F. Li, Neutrino masses, mixings and oscillations in SU(2) × U(1) models of electroweak interactions, Phys. Rev. D 22 (1980) 2860.
[11] G. Lazarides, Q. Shafi, C. Wetterich, Proton lifetime and fermion masses in an SO(10) model, Nucl. Phys. B 181 (1981) 287–300.
[12] M. Magg, C. Wetterich, Neutrino mass problem and gauge hierarchy, Phys. Lett. B 94 (1980) 61–64.
[13] J. Schechter, J.W.F. Valle, Neutrino masses in SU(2) × U(1) theories, Phys. Rev. D 22 (1980) 2227.
[14] R.N. Mohapatra, G. Senjanovic, Neutrino masses and mixings in gauge models with spontaneous parity violation, Phys. Rev. D 23 (1981) 165.
[15] A. Zee, Quantum numbers of Majorana neutrino masses, Nucl. Phys. B 264 (1986) 99–110.
[16] K.S. Babu, Model of 'calculable' Majorana neutrino masses, Phys. Lett. B 203 (1988) 132–136.
[17] K.S. Babu, C. Macesanu, Two loop neutrino mass generation and its experimental consequences, Phys. Rev. D 67 (2003) 073010, arXiv:hep-ph/0212058.
[18] D. Aristizabal Sierra, M. Hirsch, Experimental tests for the Babu–Zee two-loop model of Majorana neutrino masses, J. High Energy Phys. 12 (2006) 052, arXiv:hep-ph/0609307.
[19] M. Nebot, J.F. Oliver, D. Palao, A. Santamaria, Prospects for the Zee–Babu Model at the CERN LHC and low energy experiments, Phys. Rev. D 77 (2008) 093013, arXiv:0711.0483.
[20] D. Schmidt, T. Schwetz, H. Zhang, Status of the Zee–Babu model for neutrino mass and possible tests at a like-sign linear collider, Nucl. Phys. B 885 (2014) 524–541, arXiv:1402.2251.
[21] J. Herrero-Garcia, M. Nebot, N. Rius, A. Santamaria, The Zee–Babu model revisited in the light of new data, Nucl. Phys. B 885 (2014) 542–570, arXiv:1402.4491.
[22] A. Zee, A theory of lepton number violation, neutrino Majorana mass, and oscillation, Phys. Lett. B 93 (1980) 389.
[23] D. Aristizabal Sierra, M. Hirsch, S.G. Kovalenko, Leptoquarks: neutrino masses and accelerator phenomenology, Phys. Rev. D 77 (2008) 055011, arXiv:0710.5699.
[24] C.-S. Chen, C.Q. Geng, J.N. Ng, Unconventional neutrino mass generation, neutrinoless double beta decays, and collider phenomenology, Phys. Rev. D 75 (2007) 053004, arXiv:hep-ph/0610118.
[25] F. del Aguila, A. Aparici, S. Bhattacharya, A. Santamaria, J. Wudka, A realistic model of neutrino masses with a large neutrinoless double beta decay rate, J. High Energy Phys. 05 (2012) 133, arXiv:1111.6960.
[26] K.S. Babu, J. Julio, Two-loop neutrino mass generation through leptoquarks, Nucl. Phys. B 841 (2010) 130–156, arXiv:1006.1092.
[27] M. Gustafsson, J.M. No, M.A. Rivera, Predictive model for radiatively induced neutrino masses and mixings with dark matter, Phys. Rev. Lett. 110 (2013) 211802, arXiv:1212.4806.
[28] J. Alcaide, D. Das, A. Santamaria, A model of neutrino mass and dark matter with large neutrinoless double beta decay, J. High Energy Phys. 04 (2017) 049, arXiv:1701.01402.
[29] Y. Cai, J. Herrero-Garcia, M.A. Schmidt, A. Vicente, R.R. Volkas, From the trees to the forest: a review of radiative neutrino mass models, arXiv:1706.08524.
[30] ATLAS collaboration, G. Aad, et al., Inclusive search for same-sign dilepton signatures in pp collisions at $\sqrt{s} = 7$ TeV with the ATLAS detector, J. High Energy Phys. 10 (2011) 107, arXiv:1108.0366.
[31] ATLAS collaboration, G. Aad, et al., Search for new phenomena in events with three charged leptons at $\sqrt{s} = 7$ TeV with the ATLAS detector, Phys. Rev. D 87 (2013) 052002, arXiv:1211.6312.
[32] ATLAS collaboration, G. Aad, et al., Search for doubly-charged Higgs bosons in like-sign dilepton final states at $\sqrt{s} = 7$ TeV with the ATLAS detector, Eur. Phys. J. C 72 (2012) 2244, arXiv:1210.5070.
[33] CMS collaboration, S. Chatrchyan, et al., A search for a doubly-charged Higgs boson in pp collisions at $\sqrt{s} = 7$ TeV, Eur. Phys. J. C 72 (2012) 2189, arXiv:1207.2666.
[34] ATLAS collaboration, Search for Doubly-Charged Higgs Bosons in Same-Charge Electron Pair Final States Using Proton–Proton Collisions at $\sqrt{s} = 13$ TeV with the ATLAS Detector, Tech. Rep. ATLAS-CONF-2016-051, 2016.
[35] CMS collaboration, A Search for Doubly-Charged Higgs Boson Production in Three and Four Lepton Final States at $\sqrt{s} = 13$ TeV, Tech. Rep. CMS-PAS-HIG-16-036, 2017.
[36] S. Kanemura, K. Yagyu, H. Yokoya, First constraint on the mass of doubly-charged Higgs bosons in the same-sign diboson decay scenario at the LHC, Phys. Lett. B 726 (2013) 316–319, arXiv:1305.2383.
[37] C. Englert, P. Schichtel, M. Spannowsky, Same-sign W pair production in composite Higgs models, Phys. Rev. D 95 (2017) 055002, arXiv:1610.07354.
[38] F. del Aguila, M. Chala, LHC bounds on lepton number violation mediated by doubly and singly-charged scalars, J. High Energy Phys. 03 (2014) 027, arXiv:1311.1510.
[39] J. de Blas, M. Chala, M. Perez-Victoria, J. Santiago, Observable effects of general new scalar particles, J. High Energy Phys. 04 (2015) 078, arXiv:1412.8480.
[40] F. del Aguila, M. Chala, A. Santamaria, J. Wudka, Lepton number violation and scalar searches at the LHC, Acta Phys. Pol. B 44 (2013) 2139–2148, arXiv:1311.2950.
[41] ATLAS collaboration, G. Aad, et al., Search for anomalous production of prompt same-sign lepton pairs and pair-produced doubly charged Higgs bosons with $\sqrt{s} = 8$ TeV pp collisions using the ATLAS detector, J. High Energy Phys. 03 (2015) 041, arXiv:1412.0237.
[42] CMS collaboration, Search for a Doubly-Charged Higgs Boson with $\sqrt{s} = 8$ TeV pp Collisions at the CMS Experiment, Tech. Rep. CMS-PAS-HIG-14-039, 2016.
[43] ATLAS collaboration, Search for Doubly-Charged Higgs Boson Production in Multi-Lepton Final States with the ATLAS Detector using Proton–Proton Collisions at $\sqrt{s} = 13$ TeV, Tech. Rep. ATLAS-CONF-2017-053, 2017.
[44] D. Dercks, N. Desai, J.S. Kim, K. Rolbiecki, J. Tattersall, T. Weber, CheckMATE 2: from the model to the limit, arXiv:1611.09856.
[45] ATLAS collaboration, G. Aad, et al., Search for supersymmetry at $\sqrt{s} = 13$ TeV in final states with jets and two same-sign leptons or three leptons with the ATLAS detector, Eur. Phys. J. C 76 (2016) 259, arXiv:1602.09058.
[46] CMS collaboration, A.M. Sirunyan, et al., Search for evidence of the type-III seesaw mechanism in multilepton final states in proton–proton collisions at $\sqrt{s} = 13$ TeV, arXiv:1708.07962.
[47] ATLAS collaboration, A General Search for New Phenomena with the ATLAS Detector in pp Collisions at $\sqrt{s} = 8$ TeV, Tech. Rep. ATLAS-CONF-2014-006, 2014.

[48] J. Alwall, R. Frederix, S. Frixione, V. Hirschi, F. Maltoni, O. Mattelaer, et al., The automated computation of tree-level and next-to-leading order differential cross sections, and their matching to parton shower simulations, J. High Energy Phys. 07 (2014) 079, arXiv:1405.0301.
[49] T. Sjostrand, S. Mrenna, P.Z. Skands, PYTHIA 6.4 physics and manual, J. High Energy Phys. 05 (2006) 026, arXiv:hep-ph/0603175.
[50] E. Conte, B. Fuks, G. Serret, MadAnalysis 5, a user-friendly framework for collider phenomenology, Comput. Phys. Commun. 184 (2013) 222–256, arXiv:1206.1599.
[51] R. Brun, F. Rademakers, ROOT: an object oriented data analysis framework, Nucl. Instrum. Methods 389 (1997) 81–86.
[52] A. Alloul, N.D. Christensen, C. Degrande, C. Duhr, B. Fuks, FeynRules 2.0 – a complete toolbox for tree-level phenomenology, Comput. Phys. Commun. 185 (2014) 2250–2300, arXiv:1310.1921.
[53] A.L. Read, Presentation of search results: the CL(s) technique, J. Phys. G 28 (2002) 2693–2704.
[54] T. Junk, Confidence level computation for combining searches with small statistics, Nucl. Instrum. Methods A 434 (1999) 435–443, arXiv:hep-ex/9902006.
[55] I.M. Hierro, S.F. King, S. Rigolin, Higgs portal dark matter and neutrino mass and mixing with a doubly charged scalar, Phys. Lett. B 769 (2017) 121–128, arXiv:1609.02872.